ELSEVIER

Seminars in
NUCLEAR
MEDICINE

# Update of Renal Imaging

Nicolas Grenier, MD,*,† Olivier Hauger, MD, PhD,*,† Angela Cimpean, MD,* and Vinçent Pérot, MD*

**Significant technical improvements have allowed the use of radiological techniques to play a growing role in the imaging of renal diseases. Noninvasive ultrasound methods (ie, sonography and Doppler) are now positioned as first-line methods for the evaluation of renovascular diseases. Multidetector computed tomography is able to provide high spatial resolution images of the kidneys and renal arterial vessels. Magnetic resonance imaging, which provides higher signal-to-noise ratio and higher spatial and/or temporal resolution, can display both morphological information about renal parenchyma and vessels and functional data, including perfusion, filtration, diffusion, or oxygenation. In renovascular diseases, these techniques have the potential to drive new strategies, including Doppler sonography as a first-line method, followed by computed tomography angiography or magnetic resonance angiography, depending mainly on renal function. Imaging of parenchymal renal diseases is developing toward more quantitative (volumetric and functional measurements) and more specific (through in vivo cell targeting) acquisitions for obtaining the adequate information on tissue characteristics relevant either for diagnosis or for prognosis or treatment follow-up.**


During the last few decades, significant technical improvements have allowed the use of radiological techniques to play a growing role in the imaging of renal diseases. Noninvasive ultrasound methods (sonography and Doppler) are now positioned as first-line methods for evaluation of renovascular diseases (RVDs). Multidetector computed tomography (CT) is able to provide high spatial resolution images of the kidneys and renal arterial vessels (CT angiography). Finally, magnetic resonance imaging (MRI), providing higher signal-to-noise ratio and higher spatial and/or temporal resolution, is now able to display both morphological information on renal parenchyma and vessels and functional data, such as perfusion, filtration, diffusion, or oxygenation. These techniques have the potential to create new strategies in imaging of renal diseases (as renovascular) and new opportunities for obtaining the adequate information on tissue characteristics relevant either for diagnosis or for prognosis or treatment follow-up.

*Service d'Imagerie Diagnostique et Interventionnelle de l'Adulte, Groupe Hospitalier Pellegrin, Bordeaux cedex, France.

†ERT CNRS "Imagerie Moléculaire et Fonctionnelle," Université Victor Segalen-Bordeaux 2, Bordeaux, France.

Address reprint requests to Nicolas Grenier, MD, Service d'Imagerie Diagnostique et Interventionnelle de l'Adulte, Groupe Hospitalier Pellegrin, Place Amélie Raba Léon, 33,076 - Bordeaux cedex, France. E-mail: nicolas.grenier@chu-bordeaux.fr

## Imaging of RVD

RVD is a complex entity, encompassing atherosclerotic arterial lesions, renal disease, and hypertension, leading to high renal and cardiovascular risk. The relationships among renal artery stenosis (RAS), hypertension, and renal function vary from patient to patient and are difficult to assess, but their severity and their association increase the patient's risk.[1] Atherosclerotic nephropathy is a consequence of the association of multiple factors, this multiplicity of causal factors explaining the great heterogeneity of renal damage. The radiological imaging techniques available today have to achieve 4 objectives: (1) to detect and characterize the RAS in terms of anatomical and hemodynamical severity; (2) to assess the anatomical consequences of the RAS on the artery itself and on the renal parenchyma; (3) to assess the functional and cellular consequences of the RAS on the kidney; and (4) to identify criteria of associated renal impairment related to RVD.

### Radiological Detection of RAS

Stenoses that reduce the internal diameter by >60% produce a significant decrease in renal blood flow. They can be atheromatous (60% of cases) or dysplastic (fibromuscular dysplasia, 35% of cases),[2] ostial or not ostial, and located in main, accessory, or segmental arteries.[3] The imaging techniques available are Doppler ultrasound (US), helical computed tomographic angiography (CTA), and magnetic resonance an-

0001-2998/06/$-see front matter © 2006 Elsevier Inc. All rights reserved.
doi:10.1053/j.semnuclmed.2005.08.001

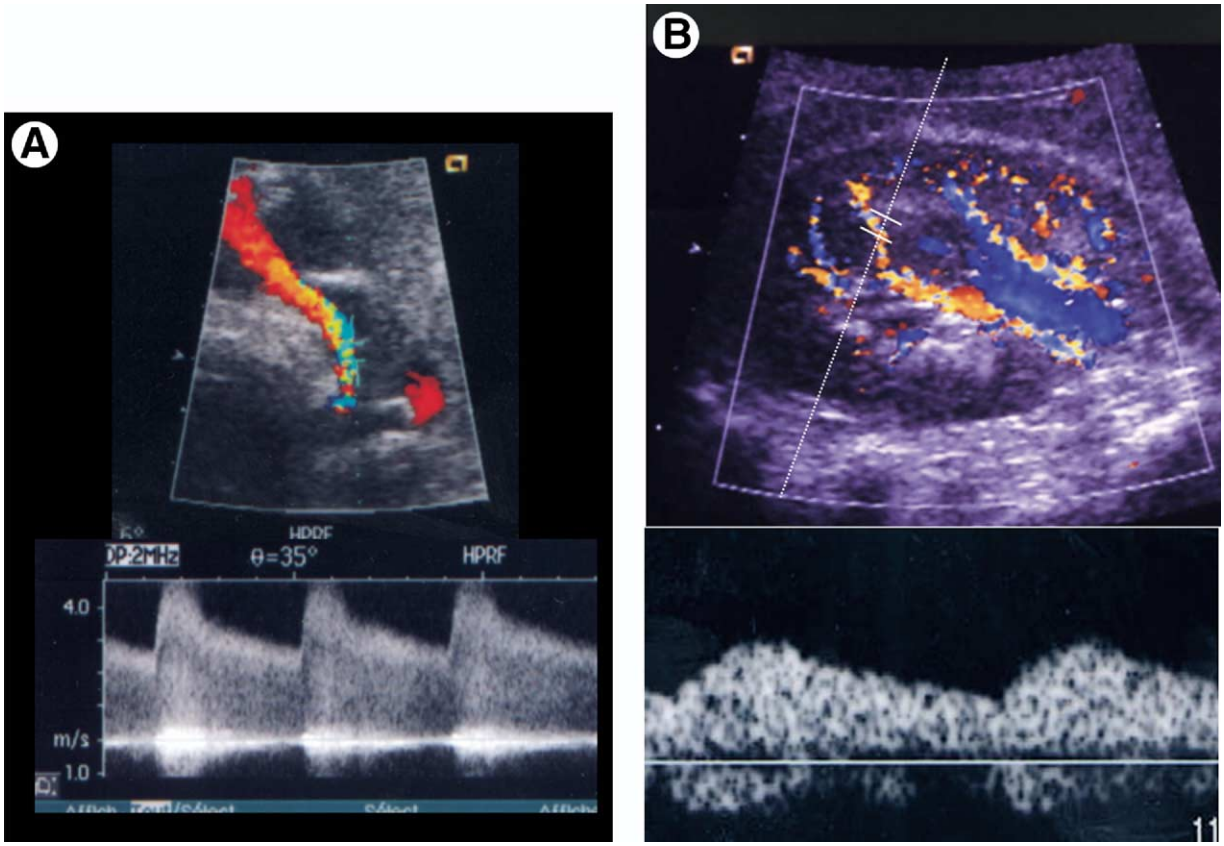


**Figure 1** Atherosclerotic stenosis of the right renal artery. (A) Direct proximal features of stenosis: Color flow sonography shows typical color changes at the ostium of right renal artery, extending in the postostial segment. Spectral sampling at the site of stenosis shows acceleration of flow (peak systolic velocity: 5 m/s) and spectral broadening. (B) Intrarenal features of severe stenosis: sampling of interlobar arteries shows a decrease of systolic acceleration with an increase of ascension time (0.173 s).

giography (MRA). Intravenous (IV) urography and IV digital subtraction angiography (DSA) are no longer recommended, and intra-arterial (IA) DSA is limited to prerevascularization planning.

## Doppler US

With the advent of color encoding of the Doppler signal, US has gained a major place in the detection of renal artery stenosis. To be of diagnostic use, a complete examination must be undertaken, including B-mode, spectral sampling, and color imaging.

The stenosis may be observed on color-flow images with focal changes of color (Fig. 1A) and/or a perivascular artifact, which are related to acceleration and turbulence, respectively. Proximal criteria of hemodynamically significant stenosis essentially are based on spectral sampling showing spectral broadening and increased velocity (Fig. 1B). The main proximal criteria used are first, a renoaortic velocity ratio greater than 3.5 for a 60% stenosis[4,5] and second, a peak systolic velocity at the site of stenosis, with an upper limit of either 150 cm/s for a 50% stenosis[6] or 180 cm/s for a 60% stenosis.[7] Using these criteria, the sensitivity and specificity of the technique compared with angiography are 89% to 98% and 90% to 98%, respectively.[7-16] Although multiple renal arteries can be detected, in all series, the detection of small accessory arteries has been reported as very low.

Severe stenoses that decrease the diameter by >75% produce distal intrarenal spectral changes, a tardus-parvus phenomenon with a slowed systolic acceleration and a decreased resistive index[17] (Fig 1c). Many distal quantitative criteria have been proposed in the literature (loss of early systolic peak; acceleration lower than 3 m/s$^2$; acceleration index >4, acceleration time of systolic peak >0.07 s; a difference between kidneys in resistive index of >5% or in pulsatility index of >0.12). The performance of correlative studies with angiography is confusing because of the variability in criteria and in corresponding degree of stenosis.[14,16,17-21] Interobserver and intraobserver variability using these criteria is high.[22,23] The factors responsible for changes in the distal waveforms are complex and are probably more dependent on changes of compliance than on pressure decrease.[24] Therefore, these criteria are used only when obvious on spectral traces, when quantifying the stenosis as severe (>75%), or when identifying a downstream pattern of a stenosis on a segmental or an accessory artery that has been missed.

***US Contrast Agents.*** The development of echo-enhancing agents that affect the Doppler signal has increased the sensi-

tivity of detection of flow when it is too slow or too deep. A multicenter study performed with the first commercialized agent (Levovist; Schering, Berlin, Germany; made of microbubbles of air stabilized with galactose and palmitic agent) showed that the feasibility of the US examination was increased mainly in patients with a high body mass index and in patients with decreased renal function, although neither sensitivity nor specificity were significantly improved.[8]

***Doppler With Captopril.*** To overcome the lack of sensitivity of distal criteria for detecting proximal RAS, the administration of captopril has been proposed,[21,25] as a "stress test": captopril produces a vasodilatation and, when a proximal stenosis is present, increases the pulsus-tardus phenomenon, giving complete sensitivity and specificity for diagnosis of 50% RAS. Its use in daily practice is not recommended.

### CTA

The use of slip-ring CT scanners capable of contiguous tube rotations coupled with continuous table incrementation allows for the volumetric acquisition of imaging data from the abdominal aorta, including renal arteries, during a single breath hold. With single-ring CT scanners, Rubin and coworkers[26] showed that maximum intensity projections provided better sensitivity (92%) than surface shaded display (59%). However, Johnson and coworkers[27] reported that the volume rendering technique provided a better specificity (99%) than maximum intensity projection (87%). Performance of CTA in detecting significant stenoses is good with high sensitivity (88-96%), high specificity (83-99%),[28-30] and close correlation with angiography for grading stenoses.[30] The detection of accessory arteries is much better than with Doppler US (average 90%). CT also shows the exact nature of stenoses, eg, ostial, truncal or pseudotruncal[31] and the degree of calcification of lesions before endovascular treatment.

With multislice CT, which allows between 4 and 16 slices per rotation, the axial resolution is improved, approaching 1-mm slice thickness (Fig. 2), and the amount of iodinated contrast agent can be reduced. Because of a better spatial resolution, the separation of calcification and true lumen is more accurate,[32] and distal lesions, as fibromuscular dysplasia, are better delineated. Preliminary results of this technique are extremely encouraging, but comparative studies with angiography are still not available.

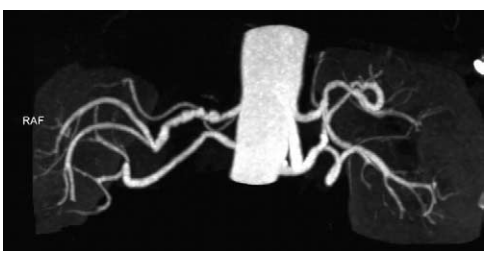


**Figure 2** Typical fibromuscular dysplasia of 1 of the 2 right renal arteries imaged with a 16-rings contrast-enhanced spiral CT angiography on a coronal maximum intensity projection.

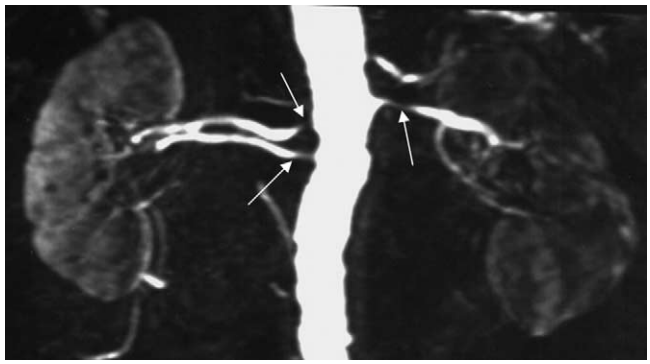

**Figure 3** 3D Gd-enhanced MRA of the abdominal aorta with coronal maximum intensity projections showing bilateral atherosclerotic postostial stenoses (arrows) of the 2 right renal arteries and the left renal artery.

### MRA

MRA has now moved from flow-enhanced (time-of-flight or phase-contrast) sequences to T1-weighted contrast-enhanced acquisitions.[33] Its performance is excellent, with a sensitivity and specificity for diagnosis of significant stenosis between 88% and 100% and between 71% and 99%, respectively.[34-42] This technique shows the entire course of renal arteries up to the renal sinus in most cases and the complete abdominal aorta, including its bifurcation (Fig. 3). Most accessory arteries are therefore shown. The evaluation of the degree of stenosis with this method has the same interobserver variability as conventional angiography.[43] Technical improvements allow shorter acquisition times and/or higher spatial resolution.[44,45]

### Comparison of Techniques

Comparison of performance of these noninvasive tests is difficult. A recent meta-analysis[46] tried to compare the validity of CTA, MRA, and US for diagnosis of RAS in patients suspected of having RVH. Receiver-operating characteristic curves found that CTA and gadolinium (Gd)-enhanced 3-dimensional (3D) MRA performed significantly better than the other diagnostic tests and seemed to be preferred in patients referred for evaluation of RVH. However, because few studies of these tests have been published, further research is recommended.

## Anatomical and Functional Consequences of RAS

Detection of RAS requires evaluation of the severity of narrowing and its consequences on renal flow, on renal artery, on renal parenchyma and on renal function, to improve the interobserver variability and to define predictive factors of improvement after revascularization.

### Vascular Anatomy

When the stenosis is severe, a poststenotic dilation occurs as a "jet-lesion." This dilation can be used as a criterion of significant artery stenosis. This morphological change can be assessed with CTA and MRA but not with US. However, this criterion is difficult to quantify; no significant threshold has

been defined, even if a 20% dilation is widely used; it has never been evaluated to our knowledge.

### Renal Anatomy

When the renal blood flow is significantly decreased, renal parenchyma shrinks. Several parameters have been proposed to evaluate this effect. Renal length can be measured with any imaging technique. To be significant, a length difference of 1 cm should be considered, attesting of a hemodynamically significant stenosis.[47] If the renal length is less than 8 cm, revascularization is contraindicated because less likely to be of benefit.

Measurement of cortical thickness and cortical area has been proposed by Mounier-Vehier and coworkers,[48] who showed that thresholds of 8 mm for cortical thickness and of 800 $mm^2$ for cortical area allowed the differentiation of control kidneys from poststenotic kidneys, whereas renal length was still within normal range, suggesting that cortical parameters are more sensitive for early diagnosis of atherosclerotic renal disease than kidney size (Fig. 4). Cortical atrophy seems to be a useful marker for guidance in revascularization, but its prognosis value has still to be evaluated.

### Renal Hemodynamics

***Renal Arterial Flow Velocities Below the Stenosis.*** With 3D phase-contrast MRI, signal intensity within the artery becomes sensitive to flow velocity. The flow profile alteration (as with Doppler techniques) is responsible for a severe dephasing of MR signal with these sequences. It has been shown, in vitro, that the degree of spin dephasing was directly correlated with the trans-stenotic pressure gradient[49] (Fig. 4). A normal velocity-time curve is characterized by an early systolic peak (ESP), a subsequent incision, and a lower second mid-systolic peak. Schoenberg and coworkers[50,51] showed in animals and patients that either a normal curve or partial loss of the ESP were consistent with low-grade stenosis; complete loss of the ESP and decrease of the midsystolic peak indicated moderate stenosis (50%); flattened flow profile with no systolic velocity components was representative of high-grade stenosis.[52] Using this classification, the combined approach of 3D Gd-enhanced MRA and phase contrast flow sequence revealed the best interobserver variability and almost perfect intermodality agreement with DSA.

This method also allows the measurement of the renal flow rate below the stenosis (as the product of the mean velocity within the artery and the cross sectional area of renal artery). Binkert and coworkers[53] reported a renal flow index (renal flow (mL/min) divided by renal volume [$cm^3$]) less than 1.5 mL/min/$cm^3$ as predictive of successful outcome of revascularization.

***Intrarenal Hemodynamics.*** Distal intrarenal Doppler sampling for calculation of the resistive index (RI, defined as the ratio: systolic velocity − diastolic velocity/systolic velocity) can provide information about the intensity of renal consequences of RAS. Radermacher and coworkers[54] demonstrated that an increased RI > 0.8 was associated with a poor prognosis in patients with RAS shown by an absence of improvement of hypertension, renal function or kidney survival after revascularization.

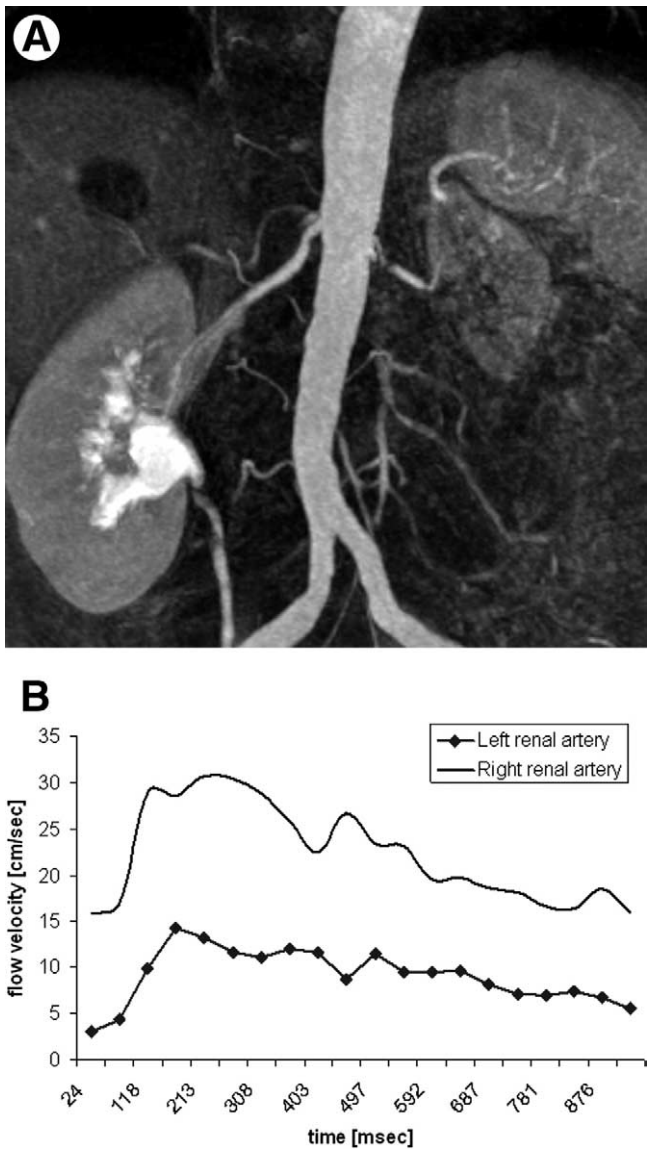


**Figure 4** Phase-contrast acquisition on renal arteries in a patient with left renal artery stenosis. (A) Example of MRA showing left renal artery stenosis with a small kidney. (B) The flow velocity-time curves, obtained on each renal artery, show a normal curve on the right with early systolic peak, and an altered flow within left renal artery without early systolic peak. (Courtesy of Dr. Stephan Schoenberg, Muenchen, Germany.)

### Renal Functional Parameters

The impact of RAS on glomerular filtration and renal perfusion has been studied with MRI.

***Captopril-Enhanced Filtration Studies.*** Gd chelates behave as glomerular tracers in the same manner as iodine contrast media. After the intravenous infusion of a bolus of Gd, it is possible to follow its intrarenal transit during breath holding. This transit begins with a vasculo-interstitial phase producing a cortical, then a medullary, enhancement of signal intensity (T1-shortening effect), a tubular phase characterized by a

drop of signal intensity (T2-shortening effect) within the external medulla that extends centripetally toward the papilla, and finally a ductal phase characterized by a late low-signal intensity within the internal medulla and the renal collecting system (Fig. 5A). In RVH, as with scintigraphy, the normal contrast kinetics are altered by captopril on the side of the stenosis, thus inducing a delay or disappearance of the tubular and ductal phases or a late T2 effect extending across the whole kidney (Fig. 5B).[55]

***Renal Perfusion.*** The degree of perfusion depends on both the arterial flow rate and local factors, such as regional blood volume and vasoreactivity. Theory of perfusion calculation as well as imaging methods depends on the type of contrast agent used. Absolute quantification of parenchymal perfusion can be assessed with diffusible (as Gd-chelates)[56] or purely intravascular contrast agents (as iron oxide particles).[57] However, nondiffusible tracers are still not permitted for clinical use.

The most widely used perfusion model, with Gd chelates, is derived from Peters's model. Introducing the arterial changes of R1 ($\Delta R1_{art}$), calculation of renal perfusion per unit of volume can be extracted from the mathematical expression:

$$RBF/vol = \max slope_{renal} / \max \Delta R1_{art}$$

Renal perfusion can alternatively be measured using pulsed arterial spin labeling (or spin-tagging) using endogenous water as a diffusible tracer.[58] With this technique, a perfusion-weighted image can be generated by the subtraction of an image in which inflowing spins have been labeled from an image in which spin labeling has not been performed. Quantitative perfusion maps can then be calculated (in mL/min/100 g of tissue) when T1 of the tissue and efficiency of labeling are known.

A 50% decrease of cortical perfusion (from 400 mL/min/100g to 200 mL/min/100g) has been observed after a tight (80%) stenosis; however, atherosclerotic nephropathy, because of its vascular components, also can be responsible for a decrease of perfusion to 180 mL/min/100 g.[57] Distinction between these 2 types of cortical perfusion changes have not been demonstrated.

***Other Functional Parameters.*** MR imaging is able to provide other new functional parameters as a diffusion coefficients or a BOLD (Blood Oxygen Level Dependent) effect. In RAS, their results are preliminary and their significance and role in strategy still under debate. They showed a decrease of renal diffusion coefficients in patients with RAS[59] and a decreased intrarenal oxygenation during acute experimental occlusion of the renal artery in pigs.[60]

### Strategy

The best strategy to explore RVD remains a matter of debate. The choice of the best noninvasive test at present depends on the experience of each group in every technique and the availability of these techniques knowing that US is cheaper and more available than CT or MR but requires training. In good hands, it provides both criteria of significant (>60%) RAS, based on proximal hemodynamic features, and prognostic information about possibility of improvement of hypertension, renal function, or kidney survival after revascularization. If an accurate US examination is not available, or if it is inconclusive, MRA or CTA should be performed. CTA is preferred because of its greater availability, its greater spatial resolution with multi-slice systems, and its lower cost. However, MRA should be the preferred choice if the patient has impaired renal function or intolerance to iodinated contrast agents. However, "downstream damage," so-called atherosclerotic nephropathy, remains difficult to characterize whereas it represents the essential prognostic factor. The contribution of captopril-sensitized tests in this field is decreasing because the indications of reperfusion versus medical treatment are more specifically based on clinical criteria than on relation to renin-related pathophysiology. For that purpose, scintigraphy remains the gold standard, but MRI has the capacity to provide similar information.[55]

## Imaging of Nephropathies

Radiological techniques play a minor role in imaging of parenchymal nephropathies in native or in transplanted kidneys. However, acute and chronic nephropathies are responsible for morphological and functional changes of renal parenchyma. From a morphological point of view, only macroscopic changes, such as kidney size and corticomedullary differentiation, actually are used on a daily basis. From a functional point of view, scintigraphic techniques remain the major sources of renal performance assessment. Today, or in the near future, MRI may have the potential to provide important morphological and functional features for diagnosis or prognosis.

### Morphological Biomarkers of Kidney Function

There is a growing interest in validating accurate and reproducible methods for the calculation of renal volume which, may be an index of functional renal parenchyma.[61] Follow-up of chronic nephropathies would be simplified for patients by such measurements. Today, the most widely used marker is the renal length measured with sonography. However, its correlation with renal size is far from perfect.[62] The best method would be a volumetric technique, applied to the entire parenchyma, excluding the sinus, or to the cortex. Coulam and coworkers[63] reported an excellent correlation between MRI measurement of total renal parenchymal volume, done slice-by-slice, and autopsy volume and weight, using coronal multiphasic contrast-enhanced 3D sequences in pigs. In our institution, we developed an automatic segmentation technique of the renal cortex, which is directly related to filtration capabilities of the kidney, applied to a contrast-enhanced 3D data-set, obtained during the vascular phase. This technique demonstrated its feasibility (unpublished data) but still requires validation (Fig. 6).

In inherited polycystic diseases, the measurement of renal

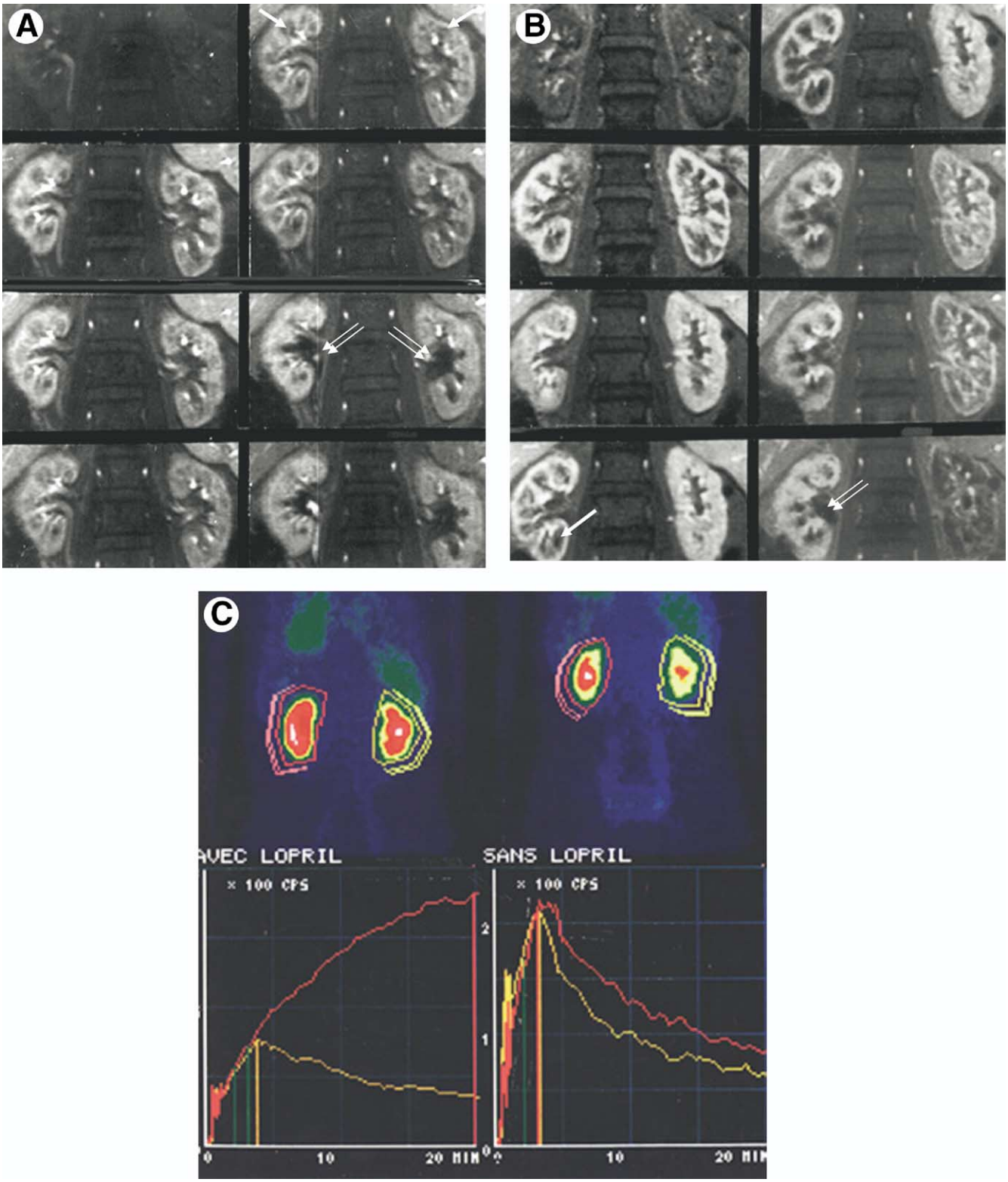


**Figure 5** Dynamic Gd-enhanced MRI of the kidneys before (A) and after (B) the administration of captopril in a patient with stenosis of the left renal artery (from top-to-bottom then left-to-right). (A) Before captopril, the tubular phase with low signal intensity within medulla (arrows) and excretion of contrast medium within renal collecting system (double arrows) are symmetrical. (B) After captopril, the right kidney shows a normal tubular phase (arrow) and normal excretion (double arrow), whereas the tubular phase is delayed on the left but then enhances with time, extending within the cortex and providing a complete low signal intensity of the left kidney; this effect is related to a severe retention of the contrast agent within the entire left kidney induced by captopril. (C) Positive captopril MAG3-Tc99 scintigraphy obtained in the same patient: the baseline study shows symmetrical elimination of the tracer (right of the image). After captopril (left of the image), there is an accumulation of the tracer within the left kidney whereas it remains unchanged in the right. (Reproduced from Grenier et al,[55] with permission from the American Journal of Roentgenology.)

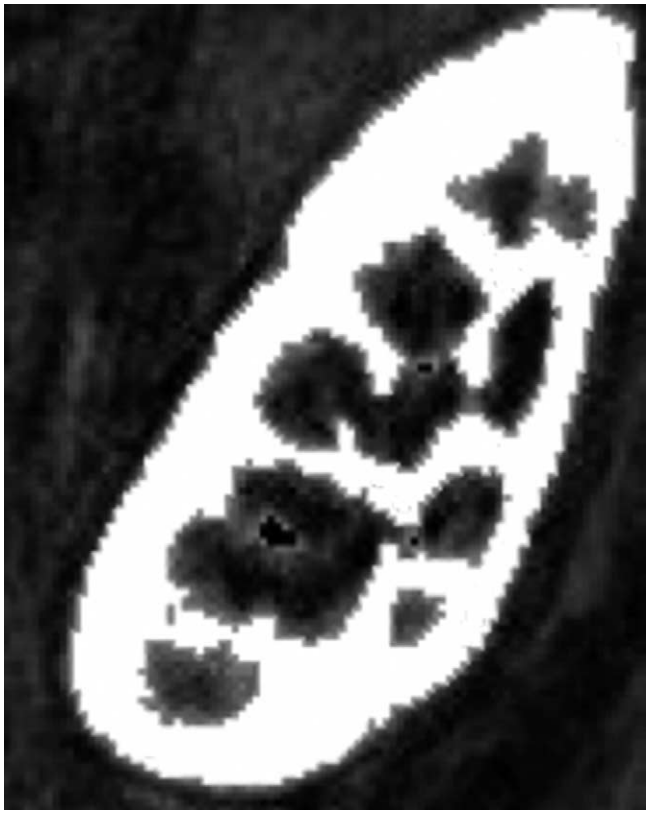

**Figure 6** Example of segmentation of the renal cortical volume, based on a contrast-enhanced 3D acquisition and on a Laplacian of a Gaussian (LoG) segmentation method.

cystic volume predicted renal outcome more reliably than total renal volume.[64] Therefore, measurement of renal cystic volume would be worthwhile to follow the effect of treatment. Computer-assisted detection software will be necessary for that purpose, with automatic detection of cyst walls and automatic volume calculation based on 3D data-sets, and used as an accurate surrogate marker, mostly when renal function is still preserved.[65]

## Functional Impact of Kidney Diseases on Filtration

### Estimation of Split Renal Function

Semiquantitative evaluation, as split renal function, usually is sufficient in urological management of most uropathies. Rohrschneider and coworkers[66] obtained calculations of the percentage of the single-kidney "activity" comparable with those derived with gamma camera scintigraphy.[67] These studies were based on a dynamic gradient-echo sequence and half of a standard clinical accepted dose of Gd-DTPA. A region of interest was positioned around the renal parenchyma (omitting medulla and pelvis), and calculation of the relative renal function was then based on the equation:

$$RF = AUC\ (mm^2) \times S\ (mm^2)$$

where AUC corresponds to the area under the a part of the time-intensity curve (Fig. 7) and S is the region of interest. The split renal function (in percentage) corresponds, for each kidney, to the product: $RF(\%) = RF/RF_{total} \times 100$, where $RF_{total}$ is the sum of RFs of both kidneys.

On the behalf of these comparable results with scintigraphy and because it is able to provide morphological and functional evaluation of the urinary tract during the same imaging session, it is likely that MRI may be used more systematically in a near future.

### Measurement of Glomerular Filtration Rate (GFR)

On the contrary, measurement of GFR is used as an index of functioning renal mass, representing the sum of filtration rates in each functioning nephron. A decrease in GFR may be the earliest and only clinical sign of renal disease, and its serial monitoring allows one to estimate the severity and to follow-up the course of kidney diseases. The measurement of GFR using MRI is a real challenge, and attempts have been unsuccessful until now. Several studies, mostly performed in animals, using different types of models showed correlation with scintigraphic techniques but with variable overestimation or underestimation.[68-71]

An extensive review of all technical problems related to quantitative GFR measurement has been published recently.[72] It requires sampling of abdominal aorta, with both kidneys, with a sufficient time resolution to accurately define the arterial input function and to separate adequately the cortical vascular phase (perfusion) and the filtration phase. Arterial signal intensity-time curve is used in different kinetic models to compensate for the noninstantaneous bolus injected into the blood. It also requires acquisition of the information within the whole kidney (and not one slice only) using fast 3D sequences. T2* effects of the contrast agent during its maximal concentration phases (intra-arterial bolus and intramedullary water reabsorption) must be minimized by a decreased injected dose and a proper selection of the parameters of the imaging sequence.

Another major problem is the necessity, for accurate quantification of these physiological parameters, to convert SI values into concentrations. Several methods, all with significant limitations, have been proposed, including scanning a phantom of tubes filled with Gd solutions at various concentrations, with the sequence used for the dynamic study, to obtain a calibration curve and a conversion equation. The solution could be to measure dynamically the R1 relaxivity instead of measuring signal intensity (based on Look-Locker sequences) because R1 is linearly correlated to tracer concentration.[73] Such approaches are still under development and validation. Finally, adequate postprocessing techniques must be used to correct for respiratory movements of the kidneys and automatic measurement of the cortical volume. If all of these requirements are overcome, and when validation is obtained with adequate goldstandards, dynamic MR will be able to provide single kidney GFR values as well as intrarenal GFR maps (Fig. 8).

These quantitative methods are still not ready to use, and many technical problems remain challenging. Therefore, scintigraphy still remains the gold standard in that field.

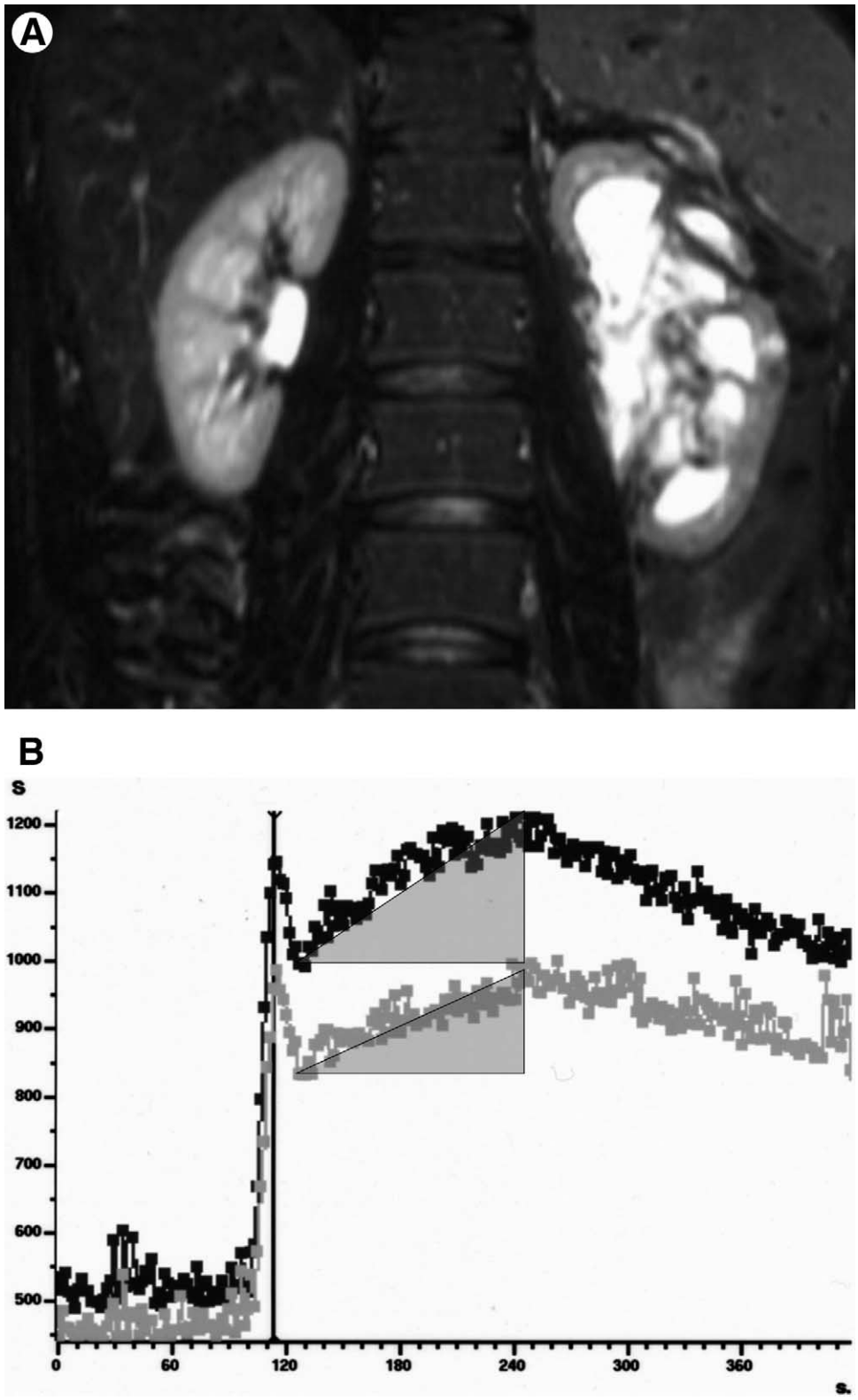


**Figure 7** Measurement of split renal function in a patient with left urinary obstruction. (A) Anatomic image showing dilation of the left pyelocaliceal system. (B) Signal intensity-time curves obtained from regions-of-interest drawn on the entire renal parenchyma (excluding pyelocaliceal system) on each side, showing 3 phases: a first abrupt ascending segment followed by a first peak, corresponding to the "vascular-to-glomerular first-pass" or cortical vascular phase; a second slowly ascending segment, ended by a second peak, corresponding to the glomerulo-tubular phase; and a slowly descending segment, corresponding to the predominant excretory function and so-called "excretory phase." Area under the curves have been drawn to calculate split renal function.

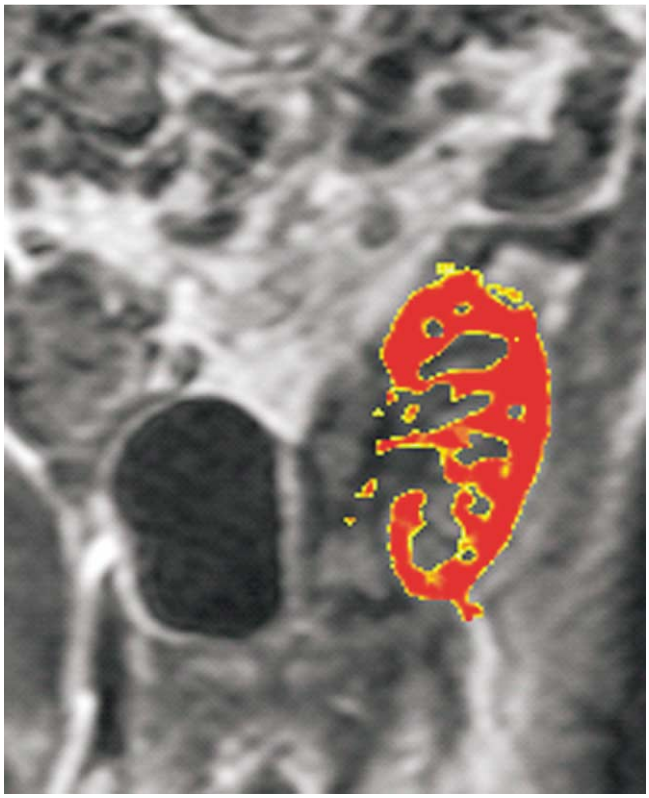

**Figure 8** GFR map of a kidney transplant obtained after dynamic T1-weighted Gd-enhanced sequence and application of the Rutland-Patlak plot on a voxel-by-voxel basis.

### Measurement of Extraction Fraction (EF)

Recently, a quantitative method of in vivo measurement of the single kidney EF was proposed by Dumoulin and coworkers[74] and implemented by Niendorf and coworkers.[75] This method is based on the measurement of T1 within flowing arterial and venous blood during slow Gd-infusion. Once the EF is calculated for each kidney, the GFR also can be calculated by measuring RBF of each renal artery using the cine-phase-contrast method. Preliminary results on animals have shown concordant results with the reference method (inulin clearance). If this quantitative method could be transposed to humans with reproducible results, the applications in nephrology would be numerous.

## Prognostic Factors of Kidney Impairment

Several physiopathological factors, considered as significant for prognosis, could be approached in the near future using specific MR techniques and specific contrast agents. These factors are medullary hypoxia, glomerular or interstitial inflammation, degree of tubule dysfunction, factors of cell viability, and the development of fibrosis.

### Medullary Hypoxia

Outer medulla is particularly sensitive to hypoxia because the active reabsorption process within the thick ascending loop of Henle requires high level of oxygen consumption.[76] Therefore, a decrease of medullary blood flow, as in acute renal failure, or an increase in tubular reabsorption, as in diabetic nephropathy (at the stage of hyperfiltration), may induce medullary hypoxia and secondary ischemia.

The blood oxygen level-dependent (ie, BOLD) technique does not measure directly $pO_2$ but allows intrarenal R2* (1/T2*) measurements, which are closely related to concentration in deoxyhemoglobin (Fig. 9).[77,78] Therefore, absolute R2* values cannot be used in practice. If the disease is asymmetric, as in renal artery stenosis, static comparison of both kidneys may identify hypoxia on one side. In renal parenchymal diseases, only dynamic changes after physiological or pharmacological manipulation can identify the kidney response.

Interestingly, diabetic subjects are unable to increase the medullary oxygenation during water diuresis. In a comparative study with a matched control group, diabetic patients without microalbuminuria, hypertension, or renal insuffi-

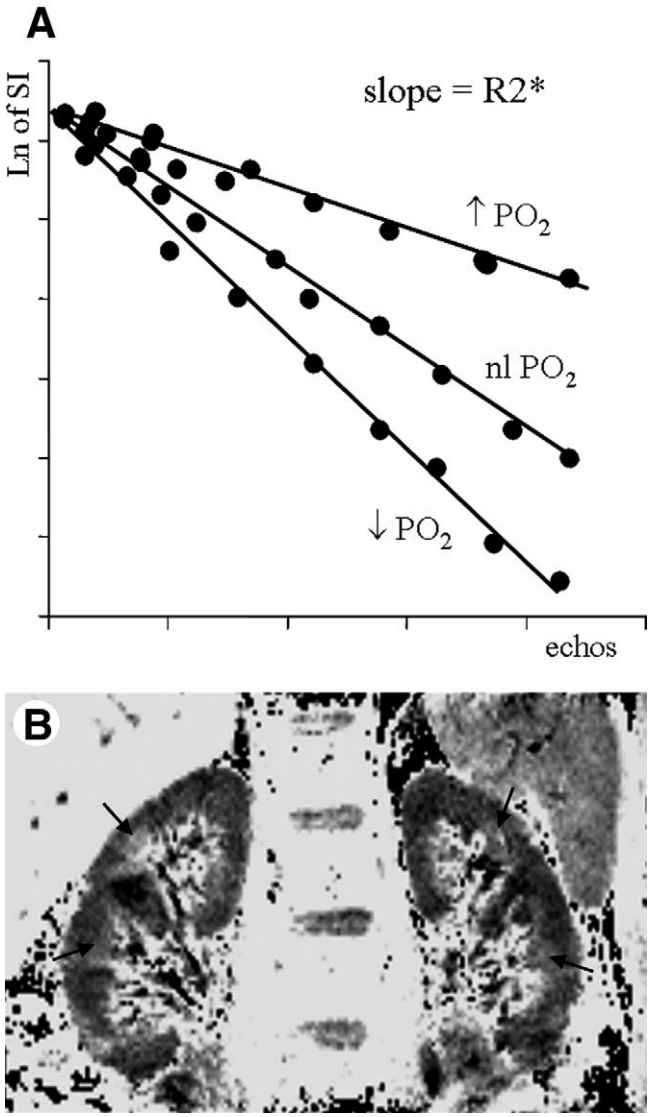


**Figure 9** Principle of blood oxygen level-dependent acquisition in the kidney. The R2* is greater when the tissue $pO_2$ is low and lower when it is high (A). A T2*-weighted multi-echo gradient echo sequence allows to calculate a R2* map showing a higher R2* value within medulla (arrows) (B).

ciency did not show any significant improvement of medullary oxygenation after water load.[79] Wider applications of this technique to clinical ischemic conditions of the medulla still have to be established.

### Intrarenal Inflammation

Macrophages, virtually absent in normal kidneys, may infiltrate renal tissues in specific nephropathies such as acute proliferative types of human and experimental glomerulonephritides, renal graft dysfunction (rejection and acute tubular necrosis), and in acute ischemic disease.[80] Their role is complex, contributing to glomerular and tubulo-interstitial injury through the secretion of various cytokines and proteases which induce changes in extra-cellular matrix and progressive fibrotic changes (glomerulosclerosis, tubulointerstitial fibrosis).

Ultra-small superparamagnetic particles of iron oxide (ie, USPIO) are small-sized nanoparticles that have a long half-life in the bloodstream (2 h in rats and 36 h in humans) and are avidly captured several hours after intravenous injection by extrahepatic cells with phagocytic activity which include blood circulating monocytes and resident macrophages that are present in most tissues.

Several models of experimental nephropathies in rats were used to demonstrate the detectability of intrarenal macrophagic activity in vivo (Fig. 10).[81-84] The degree of decrease of SI was always correlated with the number of macrophages within each renal compartment and the severity of disease. The results of the first pilot clinical study[85] seem to corroborate experimental results and justify larger multi centers clinical trials.

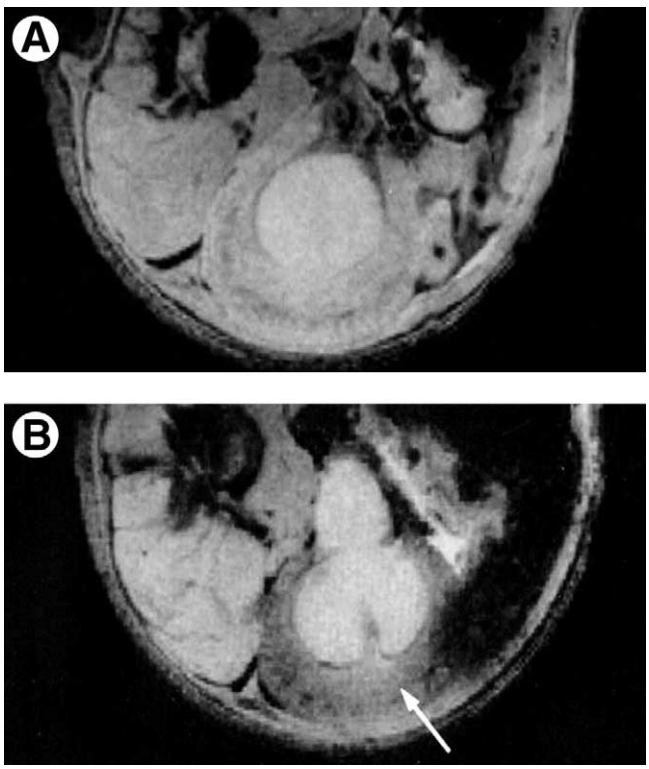


**Figure 10** Left experimental hydronephrosis in rat before (A) and 24 h after (B) the injection of USPIO. In (B), there is a notable decrease in signal intensity in the 3 renal compartments (arrow) after injection, due to the effect of superparamagnetic particles (USPIOs) phagocytized by interstitial macrophages. (Reprinted from Hauger et al,[82] with permission from the Radiological Society of North America.)

### Degree of Tubule Dysfunction

In acute renal failure models, the primary site of renal injury (proximal or distal) remains uncertain. Some authors could demonstrate proximal tubule dysfunction in acute tubular damage induced by cysplatin in mice[86] using Gd-dendrimer chelates, which are cleared by glomerular filtration.

### Cell Viability With Diffusion MRI

In acute renal failure, direct toxicity to the cells or ischemic damage may lead to apoptosis or necrosis of tubular cells. Therefore, the identification of these cellular events could help in assessing the severity and the reversibility of diseases.

SI observed on diffusion-weighted sequences depends on 2 major factors: First, on molecular movements within intracellular and extracellular spaces which depend essentially on local temperature and biological barriers present in the tissue (cellular membranes, fibers, organelles, macromolecules, etc.), and second, on "external" factors, such as perfusion, magnetic susceptibility of tissues, cardiac pulsations and respiratory movements.[87]

Using an appropriate acquisition method, cortical values of apparent diffusion coefficient (ADC) are greater in the cortex than in the medulla, and medullary diffusion is anisotropic (spatially oriented).[88] In theory, diffusion-weighted imaging could be useful to separate cellular edema, ie, reversible damage with decreased ADC values, from cellular necrosis, ie, irreversible damage with increased ADC values. In an experimental model of diabetic nephropathy, we showed that the regional ADC values were decreased within the outer medulla, when tubular cell edema occurred.[89] However, the exact role of this method in evaluating prognosis of acute renal diseases has still to be defined.

## MRI and the Development of Intrarenal Fibrosis

Exaggeration of extracellular matrix synthesis, with excessive fibrillar collagens, characterizes the development of fibrotic lesions in the glomerular, interstitial, and vascular compartments leading progressively to end-stage renal failure. This fibrotic process changes the biomechanical properties of the kidney, making quantification of these tissue changes possible with ultrasonic or MR elastography. This method requires the application of shear waves, whose propagation depends on the viscoelastic properties of the tissue; its elastic characteristics can be quantified and/or mapped as parametric images. Using MR elastography, based on a phase contrast technique that uses cyclic motion-sensitized gradients to image mechanically applied propagating acoustic shear waves, Shah and coworkers[90] validated the method in vivo on rat models of nephrocalcinosis and obtained the first elastographic images of native human kidneys.

## Cell Labeling for Follow-up of Cell Therapy

Recovery of renal function after acute nephrotoxic or ischemic insult is dependent on the replacement of necrotic tubular cells with functional tubular epithelium. This cellular regeneration originates from resident cells or from extrarenal cells. Recently, the possibility of differentiation of bone-marrow derived stem cells into mesangial cells[91] and of hematopoietic stem cells into tubular cells[92] was demonstrated in vivo, bringing great therapeutic promise for the future. Using small particles of iron oxide (ie, SPIO) preparations to magnetically label the cells, we have demonstrated the feasibility of grafting and subsequent visualization of progenitors within the kidney using either the intraarterial[93] or the intravenous route[94] for grafting.

## Acknowledgments

We thank C. Bos, J. Bulte, C. Combe, Y. Delmas, C. Deminière, B. Denis de Senneville, P. Desbarat, J. Frøkier, I. Gordon, R. Jones, CTW. Moonen, M. Pedersen, M. Ries, and J. Ripoche for their fruitful collaboration.

## References

1. Safian RD, Textor SC: Renal artery stenosis. N Engl J Med 344:431-442, 2001
2. Maxwell MH, Bleifer KH, Franklin SS, et al: Cooperative study of renovascular hypertension. Demographic analysis of the study. J Am Med Assoc 220:1195-1204, 1972
3. Beregi JP, Mauroy B, Willoteaux S, et al: Anatomic variation in the origin of the main renal arteries: Spiral CTA evaluation. Eur Radiol 9:1330-1334, 1999
4. Kohler TR, Zierler RE, Martin RL, et al: Noninvasive diagnosis of renal artery stenosis by ultrasonic duplex scanning. J Vasc Surg 4:450-456, 1986
5. Taylor DC, Kettler MD, Moneta GL, et al: Duplex ultrasound scanning in the diagnosis of renal artery stenosis: A prospective evaluation. J Vasc Surg 7:363-369, 1988
6. Hélénon O, El Rody F, Correas JM, et al: Color Doppler US of renovascular disease in native kidneys. RadioGraphics 15:833-854, 1995
7. Strandness DE: Duplex imaging for the detection of renal artery stenosis. Am J Kidney Dis 24:674-678, 1994
8. Claudon M, Plouin PF, Baxter G, et al: Renal arteries in patients at risk of renal artery stenosis : multicenter evaluation of the echo enhancer SH508A at color and spectral Doppler US. Radiology 214:739-746, 2000
9. Hua HT, Hood DB, Jensen CC, et al: The use of color flow duplex scanning to detect significant renal artery stenosis. Ann Vasc Surg 14: 118-124, 2000
10. Motew SJ, Cherr GS, Craven TE, et al. Renal duplex sonography: Main renal artery versus hilar analysis. J Vasc Surg 32:462-469; 469-471, 2000
11. De Cobelli F, Venturini M, Vanzulli A, et al: Renal arterial stenosis: prospective comparison of color Doppler US and breath-hold, three-dimensional, dynamic, gadolinium-enhanced MR angiography. Radiology 214:373-380, 2000
12. de Haan MW, Kroon AA, Flobbe K, et al: Renovascular disease in patients with hypertension: Detection with duplex ultrasound. J Hum Hypertens 16:501-507, 2002
13. Napoli V, Pinto S, Bargellini I, et al: Duplex ultrasonographic study of the renal arteries before and after renal artery stenting. Eur Radiol 12:796-803, 2002
14. Conkbayir I, Yucesoy C, Edguer T, et al: Doppler sonography in renal artery stenosis. An evaluation of intrarenal and extrarenal imaging parameters. Clin Imaging 27:256-260, 2003
15. Nchimi A, Biquet JF, Brisbois D, et al: Duplex ultrasound as first-line screening test for patients suspected of renal artery stenosis: Prospective evaluation in high-risk group. Eur Radiol 13:1413-1419, 2003
16. Stavros AT, Parker SH, Yakes WF, et al: Segmental stenosis of the renal artery: Pattern recognition of tardus and parvus abnormalities with duplex sonography. Radiology 184:487-492, 1992
17. Schwerk WB, Restrepo IK, Stellwaag M, et al: Renal artery stenosis: Grading with image-directed Doppler US evaluation of renal resistive index. Radiology 190:785-790, 1994
18. Kliewer MA, Tupler RH, Carroll BA, et al: Renal artery stenosis: Analysis of Doppler waveform parameters and tardus-parvus pattern. Radiology 189:779-787, 1993
19. Lafortune M, Patriquin HB, Demeule E, et al: Renal arterial stenosis: Slowed systole in the downstream circulation—experimental study in dogs. Radiology 184:475-478, 1992
20. Baxter GM, Aitchison F, Sheppard D, et al: Colour Doppler ultrasound in renal artery stenosis: Intrarenal waveform analysis. Br J Radiol 69: 810-815, 1996
21. Oliva VL, Soulez G, Lesage D, et al: Detection of renal artery stenosis with Doppler sonography before and after administration of captopril: Value of early systolic rise. AJR Am J Roentgenol 170:169-175, 1998
22. Kliewer MA, Tupler RH, Hertzberg BS, et al: Doppler evaluation of renal artery stenosis: Interobserver agreement in the interpretation of waveform morphology. AJR Am J Roentgenol 162:1371-1376, 1994
23. Gottlieb RH, Snitzer EL, Hartley DF, et al: Interobserver and intraobserver variation in determining intrarenal parameters by Doppler sonography. AJR Am J Roentgenol 168:627-631, 1997
24. Bude RO, Rubin JM, Platt JF, et al: Pulsus tardus: Its cause and potential limitations in detection of arterial stenosis. Radiology 190:779-784, 1994
25. René PC, Oliva VL, Bui BT, et al: Renal artery stenosis: Evaluation of Doppler US after inhibition of angiotensin-converting enzyme with captopril. Radiology 196:675-679, 1995
26. Rubin GD, Dake MD, Napel S, et al: Spiral CT of renal artery stenosis: Comparison of three-dimensional rendering techniques. Radiology 190:181-189, 1994
27. Johnson PT, Halpern EJ, Kuszyk BS, et al: Renal artery stenosis: CT angiography—comparison of real-time volume-rendering and maximum intensity projection algorithms. Radiology 211:337-343, 1999
28. Kaatee R, Beek FJA, de Lange EE, et al: Renal artery stenosis: Detection and quantification with spiral CT angiography versus optimized digital subtraction angiography. Radiology 205:121-127, 1997
29. Wittenberg G, Kenn W, Tschammler A, et al: Spiral CT angiography of renal arteries: Comparison with angiography. Eur Radiol 9:546-551, 1999
30. Van Hoe L, Vandermeulen D, Gryspeerdt S, et al: Assessment of accuracy of renal artery stenosis grading in helical CT angiography using maximum intensity projections. Eur Radiol 6:658-664, 1996
31. Kaatee R, Beek FJA, Verschuyl EJ, et al: Renal artery stenosis: Detection and quantification with spiral CT angiography versus optimized digital subtraction angiography. Radiology 199:637-640, 1996
32. Fleischmann D. Multiple detector-row CT angiography of the renal and mesenteric vessels. Eur J Radiol 45:S79-S87, 2003 (suppl 1)
33. Prince MR, Narasimhan DL, Stanley JC, et al: Breath-hold Gadolinium-enhanced MR angiography of the abdominal aorta and its major branches. Radiology 197:785-792, 1995
34. Rieumont MJ, Kaufman JA, Geller SC, et al: Evaluation of renal artery stenosis with dynamic gadolinium-enhanced MR angiography. AJR Am J Roentgenol 169:39-44, 1997
35. Hany TF, Debatin JF, Leung DA, et al: Evaluation of the aortoiliac and renal arteries: Comparison of breath-hold, contrast-enhanced, three-dimensional MR angiography with conventional catheter angiography. Radiology 204:357-362, 1997
36. De Cobelli F, Vanzulli A, Sironi S, et al: Renal artery stenosis : evaluation with breath-hold, three-dimensional, dynamic, gadolinium-enhanced versus three-dimensional, phase-contrast MR angiography. Radiology 205: 689-695, 1997
37. Tello R, Thomson KR, Witte D, et al: Standard dose Gd-DTPA dynamic MR of renal arteries. J Magn Reson Imaging 8:421-426, 1998

38. Bakker J, Beek FJA, Beutler JJ, et al: Renal artery stenosis and accessory renal arteries : accuracy of detection and visualization with Gadolinium-enhanced breath-hold MR angiography. Radiology 207:497-504, 1998
39. Thornton J, O'Callaghan J, Walshe J, et al: Comparison of digital subtraction angiography with gadolinium-enhanced magnetic resonance angiography in the diagnosis of renal artery stenosis. Eur Radiol 9:930-934, 1999
40. Völk M, Strotzer M, Lenhart M, et al: Time-resolved contrast-enhanced MR angiography of renal artery stenosis: diagnostic accuracy and inter-observer variability, AJR Am J Roentgenol 174:1583-1588, 2000
41. Fain SB, King BF, Breen JF, et al:. High-spatial resolution contrast enhanced MR angiography of the renal arteries: A prospective comparison with digital subtraction angiography, Radiology 218:481-490, 2001
42. Wilman AH, Riederer SJ, King BF, et al: Fluoroscopically triggered contrast-enhanced three-dimensional MR angiography with elliptical centric view order: Application to the renal arteries. Radiology 205: 137-146, 1997
43. Gilfeather M, Yoon HC, Siegelman ES, et al: Renal artery stenosis: Evaluation with conventional angiography versus Gadolinium-enhanced MR angiography. Radiology 210:367-372, 1999
44. Masunaga H, Takehara Y, Isoda H, et al: Assessment of gadolinium-enhanced time-resolved three-dimensional MR angiography for evaluating renal artery stenosis. AJR Am J Roentgenol 176:1213-1219, 2001
45. Breath-hold contrast-enhanced three-dimensional MR angiography of the abdomen: time-resolved imaging versus single-phase imaging, Radiology 214:149-156, 2000
46. Vasbinder GB, Nelemans PJ, Kessels AG, et al: Diagnostic tests for renal artery stenosis in patients suspected of having renovascular hypertension: A meta-analysis. Ann Intern Med 18; 135:401-411, 2001
47. Zhang HL, Schoenberg SO, Resnick LM, et al: Diagnosis of renal artery stenosis: combining gadolinimum-enhanced three-dimensional magnetic resonance angiography with functional magnetic resonance pulse sequences. Am J Hypertens 16:1079-1082, 2003
48. Mounier-Vehier C, Lions C, Devos P, et al: Cortical thickness: An early morphological marker of atherosclerotic renal disease. Kidney Int 61: 591-598, 2002
49. Mustert BR, Williams DM, Prince MR: In vitro model of arterial stenosis: Correlation of MR signal dephasing and trans-stenotic pressure gradients. Magn Reson Imaging 16:301-310, 1998
50. Schoenberg SO, Knopp MV, Bock M, et al: Combined morphologic and functional assessment of renal artery stenosis using gadolinium enhanced magnetic resonance imaging. Nephrol Dial Transplant 13: 2738-2742, 1998
51. Schoenberg SO, Bock M, Kallinowski F, et al: Correlation of hemodynamic impact and morphologic degree of renal artery stenosis in a canine model. J Am Soc Nephrol 11:2190-8, 2000
52. Schoenberg SO, Knopp MV, Londy F, et al. Morphologic and functional magnetic resonance imaging of renal artery stenosis: a multireader tricenter study. J Am Soc Nephrol 13:158-169, 2002
53. Binkert CA, Debatin JF, Schneider E, et al. Can MR measurement of renal artery flow and renal volume predict the outcome of percutaneous transluminal renal angioplasty? Cardiovasc Intervent Radiol 24: 233-239, 2001
54. Radermacher J, Chavan A, Bleck J, et al: Use of Doppler ultrasonography to predict the outcome of therapy for renal-artery stenosis. N Engl J Med 344:410-417, 2001
55. Grenier N, Trillaud H, Combe C, et al: Diagnosis of renovascular hypertension with captopril-sensitized dynamic MR of the kidney: Feasability and comparison with scintigraphy. AJR Am J Roentgenol 166: 835-843, 1996
56. Vallee JP, Lazeyras F, Khan HG, et al: Absolute renal blood flow quantification by dynamic MRI and Gd-DTPA. Eur Radiol 10:1245-1252, 2000
57. Schoenberg SO, Aumann S, Just A, et al: Quantification of renal perfusion abnormalities using an intravascular contrast agent (part 2): Results in animals and humans with renal artery stenosis. Magn Reson Med 49:288-98, 2003
58. Calamante F, Thomas DL, Pell GS, et al: Measuring cerebral blood flow using magnetic resonance imaging techniques. J Cereb Blood Flow Metab 19:701-735, 1999
59. Namimoto T, Yamashita Y, Mitsuzaki K, et al: Measurement of the apparent diffusion coefficient in diffuse renal disease by diffusion-weighted echo-planar MR imaging. J Magn Reson Imaging 9:832-837, 1999
60. Juillard L, Lerman LO, Kruger DG, et al: Blood oxygen level-dependent measurement of acute intra-renal ischemia. Kidney Int 65:944-950, 2004
61. Saxena AB, Busque S, Arjane P, et al: Preoperative renal volumes as a predictor of graft function in living donor transplantation. Am J Kidney Dis 44:877-85, 2004
62. Bakker J, Olree M, Kaatee R, et al: Renal volume measurements: Accuracy and repeatability of US compared with that of MR imaging. Radiology 211:623-628, 1999
63. Coulam CH, Bouley DM, Sommer FG: Measurement of renal volumes with contrast-enhanced MRI. J Magn Reson Imaging 15:174-179, 2002
64. King BF, Reed JE, Bergstralh EJ, et al: Quantification and longitudinal trends of kidney, renal cyst, and renal parenchyma volumes in autosomal dominant polycystic kidney disease. J Am Soc Nephrol 11:1505-1511, 2000
65. Chapman AB, Guay-Woodford LM, Grantham JJ, et al: Renal structure in early autosomal-dominant polycystic kidney disease (ADPKD): The Consortium for Radiologic Imaging Studies of Polycystic Kidney Disease (CRISP) cohort. Kidney Int 64:1035-1045, 2003
66. Rohrschneider WK, Haufe S, Wiesel M, et al: Functional and morphologic evaluation of congenital urinary tract dilatation by using combined static-dynamic MR urography: Findings in kidneys with a single collecting system. Radiology 224:683-694, 2002
67. Rohrschneider WK, Haufe S, Clorius JH, et al: MR to assess renal function in children. Eur Radiol 13:1033-1045, 2003
68. Baumann D, Rudin M: Quantitative assessment of rat kidney function by measuring the clearance of the contrast agent Gd(DOTA) using dynamic MRI. Magn Reson Imaging 18:587-595, 2000
69. Laurent D, Poirier K, Wasvary J, et al: Effect of essential hypertension on kidney function as measured in rat by dynamic MRI. Magn Reson Med 47:127-134, 2002
70. Hackstein N, Heckrodt J, Rau WS: Measurement of single-kidney glomerular filtration rate using a contrast-enhanced dynamic gradient-echo sequence and the Rutland-Patlak plot technique. J Magn Reson Imaging 18:714-725, 2003
71. Annet L, Hermoye L, Peeters F, et al: Glomerular filtration rate: assessment with dynamic contrast-enhanced MRI and a cortical-compartment model in the rabbit kidney. J Magn Reson Imaging 20:843-849, 2004
72. Huang AJ, Lee VS, Rusinek H: MR imaging of renal function. Radiol Clin North Am 41:1001-1017, 2003
73. Pedersen M, Dissing T, Deding D, et al. MR renography based on contrast-enhanced T1-mapping. Presented at the International Society for Magnetic Resonance in Medicine, Miami, Fl, May 7-13, 2005
74. Dumoulin CL, Buonocore MH, Opsahl LR, et al: Noninvasive measurement of renal hemodynamic functions using gadolinium enhanced magnetic resonance imaging. Magn Reson Med 32:370-378, 1994
75. Niendorf ER, Grist TM, Lee FT Jr, et al: Rapid in vivo measurement of single-kidney extraction fraction and glomerular filtration rate with MR imaging. Radiology 206:791-798, 1998
76. Brezis M, Rosen S: Hypoxia of the renal medulla–its implications for disease. N Engl J Med 332:647-655, 1995
77. Prasad PV, Chen Q, Goldfarb JW, et al: Breath-hold R2* mapping with a multiple gradient-recalled echo sequence: Application to the evaluation of intrarenal oxygenation. J Magn Reson Imaging 7:1163-1165, 1997
78. Prasad PV, Edelman RR, Epstein FH: Noninvasive evaluation of intrarenal oxygenation with BOLD MRI. Circulation 94:3271-3275, 1996
79. Economides PA, Caselli A, Zuo CS, et al: Kidney oxygenation during water diuresis and endothelial function in patients with type 2 diabetes and subjects at risk to develop diabetes. Metabolism 53:222-227, 2004
80. Erwig LP, Kluth DC, Rees AJ: Macrophages in renal inflammation. Curr Opin Nephrol Hypertens 10:341-347, 2001

81. Hauger O, Delalande C, Trillaud H, et al: MR imaging of intrarenal macrophage infiltration in an experimental model of nephrotic syndrome. Magn Reson Med 41:156-162, 1999
82. Hauger O, Delalande C, Deminiere C, et al: Nephrotoxic nephritis and obstructive nephropathy: Evaluation with MR imaging enhanced with ultrasmall superparamagnetic iron oxide-preliminary findings in a rat model. Radiology 217:819-826, 2000
83. Ye Q, Yang D, Williams M, et al: In vivo detection of acute rat renal allograft rejection by MRI with USPIO particles. Kidney Int 61:1124-1135, 2002
84. Jo SK, Hu X, Kobayashi H, et al: Detection of inflammation following renal ischemia by magnetic resonance imaging. Kidney Int 64:43-51, 2003
85. Hauger O, Grenier N, Deminière C, et al. Late Sinerem-enhanced MR imaging of renal diseases: A pilot study. Radiology 233(P):512, 2004
86. Kobayashi H, Kawamoto S, Jo SK, et al: Renal tubular damage detected by dynamic micro-MRI with a dendrimer-based magnetic resonance contrast agent. Kidney Int 61:1980-1985, 2002
87. Murtz P, Flacke S, Traber F, et al: Abdomen: Diffusion-weighted MR imaging with pulse-triggered single-shot sequences. Radiology 224: 2582–2564, 2002
88. Ries M, Jones RA, Basseau F, et al: Diffusion tensor MRI of the human kidney. J Magn Reson Imaging 14:42-49, 2001
89. Ries M, Basseau F, Tyndal B, et al: Renal diffusion and BOLD MRI in experimental diabetic nephropathy. Blood oxygen level-dependent. J Magn Reson Imaging 17:104-113, 2003
90. Shah NS, Kruse SA, Lager DJ, et al: Evaluation of renal parenchymal disease in a rat model with magnetic resonance elastography. Magn Reson Med 52:56-64, 2004
91. Imasawa T, Utsunomiya Y, Kawamura T, et al: The potential of bone marrow-derived cells to differentiate to glomerular mesangial cells. J Am Soc Nephrol 12:1401-1409, 2001
92. Lin F, Cordes K, Li L, et al: Hematopoietic stem cells contribute to the regeneration of renal tubules after renal ischemia-reperfusion injury in mice. J Am Soc Nephrol 14:1188-1199, 2003
93. Bos C, Delmas Y, Desmouliere A, et al: In vivo MR imaging of intravascularly injected magnetically labeled mesenchymal stem cells in rat kidney and liver. Radiology 233:781-789, 2004
94. Hauger O, Frost EE, Deminière C, et al. MR evaluation of the glomerular homing of magnetically labeled mesenchymal stem cells in a rat model of nephropathy. Radiology (in press)